NUMERICAL ANALYSIS OF COOLING AN ELECTRONIC CIRCUIT COMPONENT WITH CROSS FLOW AND JET COMBINATION

T. Demircan

Department of Mechanical Engineering
Faculty of Engineering, Kırıkkale University
Kırıkkale, Turkey

ABSTRACT

In this study, cooling of a constant temperature cube that represents electronic components inserted inside a channel are investigated. For this purpose, primary air with constant velocity is transferred from channel input, and secondary air with impinging jet is transferred to channel upper surface which corresponds to top part of the components. The flows are in contact with the cube that has constant temperature and effects the thermal boundary layer on the cube surfaces to create a heat transfer from cube to fluid. This situation is simulated under turbulence conditions for different values of nozzle jet input velocity (V_j) and channel input velocity (U_c) using Reynolds number between 30000-90000 based on channel input velocity. For this purpose, velocity, temperature, and pressure distributions are obtained for the solution region using CFD package program. As a result, flow and thermal characteristics inside the channel are parametrically calculated based on Reynolds number, Nusselt number, and cube surface temperature.

Keywords: Cross flow, Cooling electronic, Impinging jet, CFD.

1. INTRODUCTION

Considering the current technological environment, the need for electronic components are increasing. In line with technological developments, the size of electronic circuit components is decreasing. On the other hand, processor speeds and functions are evolving. In this sense, the heat dissipation of these components is parallelly increasing. The increase in heat dissipation causes the need for more effective cooling techniques. Current cooling techniques transfers cooling fluids above the electronic components via fan and the systems are cooled accordingly. Yet, a standard electronic circuit board contains multiple, heat dissipating electronic components. The components have different heat generation properties. Therefore, the surface temperatures can have different values. Standard cooling using a fan could be sufficient to cool certain electronic components that generate heat. Yet, this cooling structure can be insufficient to cool down certain electronic components.

For this purpose, researchers had developed cooling technique using an impinging jet which cools the components by spraying cooling fluids in high velocity. Impinging jets are commonly used in many industrial applications namely in systems that has electronic components with high heat flux. Colling with impinging jet provides a local cooling. When the jet impinges the surface, the jet creates a high, local heat transfer, yet the effect fades away in other surfaces. Thus, effective cooling of all components of electronic circuit may not be obtained.

As is seen, channel cooling and imping jet cooling techniques can have certain advantages and disadvantages. Combining low velocity channel flow and local high velocity imping jet can decrease the disadvantages. Thus, when combining these two methods in cooling the electronic circuit components is considered, an effective cooling operation can be obtained throughout all system components.

In literature, there are various techniques and studies regarding cooling electronic components that generate heat and keeping these components within secure temperature limits. Different cooling techniques, geometric structures, flow conditions, flow, and thermal characteristics of these studies were investigates and parameters that will affect heat transfer were analysed [1-3]. Similarly, there are studies related to cooling electronic components with impinging jet, in-channel flow, and cross flow. Most of these researches focus on only impinging jets or impinging with different Reynolds numbers on axisymmetric circular two cross flows on a flat surface or the ratio between changing the nozzle-impinging surface distance and jet diameter (H/D). Rundström and Moshfegh [4] investigated thermal performance changes

* Corresponding author (tolgademircan@gmail.com)

DOI : 10.1017/jmech.2018.11
Copyright © 2018 The Society of Theoretical and Applied Mechanics
https://doi.org/10.1017/jmech.2018.11 Published online by Cambridge University Press

of a system with a constant temperature cube which was cooled with channel flow when a circular impinging jet is added. It is observed that all simulations regarding cross flow velocity chances increased average heat transfer coefficient of the cube surface as the jet velocity increases. Meinders *et al*. [5] experimentally investigated successive one or multiple blocks mounted on a surface parallel to flow axis in terms of flow regions, flow circulation on the opposite direction of block flow, temperature, and convection effects. The results indicated that flow under low Reynolds numbers was natural convection while higher Reynold numbers created flow dispersion on the top surface of the block and the flow had irregular structure.

Lee and Lee [6] investigated flow distribution on the surface and Nusselt numbers by using circular impinging jet flow liquid crystal technique on a constant heat flux flat surface. Mergen [7] investigated the effect of an impinging jet using a nozzle on the heat transfer of a constant heat dissipating electronic component located in the middle of a rectangular cross-sectional channel. It is observed that as H/D ratio decreases, average Nusselt numbers on the surfaces decreases, and as jet and channel Reynolds numbers increases, heat convection increases. Ostheimer and Yang [8] numerically investigated twin impinging jet transferred inside a cross flow using computational fluid dynamics. Simulations were conducted using k-ε model and RSM approach and the results are investigated using the experimental data. Guoneng *et al*. [9] experimentally investigated heat transfer on a flat plate combining multiple impinging jet and cross flow. The experiment results are used for developing empirical equations.

Hayee *et al*. [10] experimentally and numerically investigated impinging jet flows and heat transfer characteristics on a short jet to plate distance jet sequences inside a cross flow. The peak value of Nusselt number was observed as the cross-flow velocity increases. Local maxima for Nusselt number is determined when the jet velocity and cross flow velocity ratio is 3. Qi *et al*. [11] experimentally and numerically investigated vertical, two dimensional, and turbulence jet flow structure inside a cross flow. Combining impinging jet and cross flow created a stronger turbulence. Rundström and Moshfegh [12] investigated flow and thermal characteristic of cross flow and impinging jet configuration of a cube mounted on a heated wall suing large-eddy simulation (LES) method. The results showed that impinging jet had better results in stagnation region in LES compared to RSM. Popovac and Hanjalic [13] numerically investigated flow caused by application of cross flow and impinging jet applications on 5 heated cube inserted on the bottom surface of a planar channel.

Chiang [14] applied impinging jet on a parallel-plain fin heat sink for an experimental study and developed optimum design parameters for the geometry. Magharabie *et al*. [15] numerically investigated cooling the sequential heated barriers using cross flow and impinging jet configuration. As Re_j/Re_c ratio increases, average Nusselt number of the bottom surfaces of the barriers increased and the average Nusselt number of the top surfaces decreased. Heo *et al*. [16] developed a curved elliptic impinging jet heat transfer inside a cross flow and determined optimum geometry and operating conditions. As a result, the area-averaged Nusselt number was increased 7.89% compared to first condition. Shapiro *et al*. [17] experimentally investigated caustic control optimization of a cross impinging circular gas jet inside cross flow. Yakhot *et al*. [18] investigated the flow and flow characteristics of a cube inserted in a turbulence channel using direct numerical simulation (DNS). The authors stated that vortex and circulation structure was observed inside the flow. Popovac *et al*. [19] numerically investigated flow and thermal characteristics of a cube inserted on a surface by combining impinging jet and cross flow. Vortex and circulation were observed in the flow region and these factors effected the boundary layer and the heat transfer was increased.

In this study, a problem that combines channel flow cooling and impinging jet cooling to cool down a heat dissipating cube which is a repetition of the electronic components. The purpose of this approach is to cool the all thermal components of an electronic circuit at certain level using primary flow and by applying impinging jet to high thermal load components, supporting the local cooling activities of the related elements and providing safe operating temperatures for all thermal components. For this purpose, one of the electronic circuit components is represented as a cube and the cooling process of this component was simulated.

2. DEFINITION OF THE PROBLEM

In this study, cooling of a constant temperature cube that represents electronic components inserted inside a channel is investigated. Figure 1 shows the schematic representation of the problem.

As the figure suggest, geometric structure adopted in Meinders *et al*. [5] was selected as basis. The schematic consists of a rectangular cross-sectional channel, a heat dissipating cube block in the middle of this channel, and a layer with low thermal conductivity around this block. Primary air has constant velocity at the channel input and the air is transferred to the channel output by transferring the heat on the cube. Simultaneously,

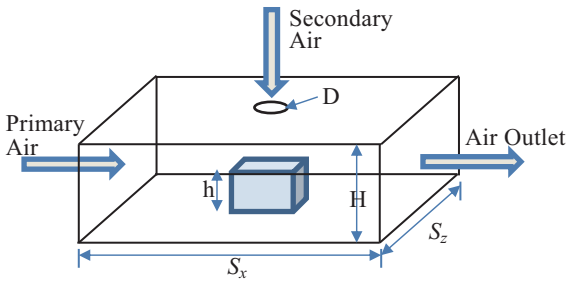


Fig. 1 Schematic representation of the problem.

https://doi.org/10.1017/jmech.2018.11 Published online by Cambridge University Press

Table 1 Geometric dimensions of the problem.

D	12 mm
h	15 mm
H	51 mm
S_x	60 mm
S_z	60 mm

Table 2 Material properties.

	Air	Epoxy	Copper
C_p	1006.1	1668.5	381
ρ	1.2047	1150	8978
λ	0.025596	0.24	387.6
μ	1.8205e-05	-	-

secondary air is impinged at a higher constant velocity on the cube which is had a circular nozzle impinging jet structure on the top surface of the channel and the surfaces of the cube are cooled. The core of the cube block is accepted as a 70°C constant temperature copper material and the cube is coated with a 1.5 mm thick epoxy layer.

Table 1 shows the geometric dimensions of the problem. In this table, the abbreviations are represented as follows: "H" is the height, "S_x" is the length, "S_z" is the width, "D" is the diameter of the jet nozzle, and "h" is the height of the block.

The temperatures of primary air from channel input and secondary air from nozzle on the channel top surface is 20°C. Epoxy layer surrounding the block consists of a low thermal conductive material. Properties of air, copper, and epoxy layers (for 70°C) adopted in this study are shown in Table 2.

In this table the abbreviations are represented as follows: "C_p" is the specific heat (J/kgK), "ρ" is material density (kg/m^3), "λ" is material heat conductivity (W/mK), and "μ" is material viscosity (kg/ms). In addition, gravitational acceleration and heat transfer with radiation are omitted. The change in fluid density, viscosity, and heat conductivity are omitted. All surface of the channel is isolated.

3. MATHEMATICAL FORMULATION

The problem investigated in this study is steady, three dimensional, non-compressible, and has turbulence. Additionally, there is zero heat generation inside the solution region. To obtain temperature, pressure, and velocity distributions of the problem, differential equations should be solves using boundary conditions. Differential equations of the problem are given below.

3.1 Differential Equations

3.1.1 Continuity Equation

$$\frac{\partial \overline{u}_j}{\partial x_j} = 0 \tag{1}$$

3.1.2 Momentum Equations

$$\frac{\partial}{\partial x_j}(\overline{u}_j\overline{u}_j) = f_i - \frac{1}{\rho}\frac{\partial \overline{p}}{\partial x_i} + \frac{\partial}{\partial x_j}\left[\frac{\mu}{\rho}\left(\frac{\partial \overline{u}_i}{\partial x_j} + \frac{\partial \overline{u}_j}{\partial x_i}\right)\right] + \frac{1}{\rho}\frac{\partial}{\partial x_j}\left(-\rho\overline{u}_i'\overline{u}_j'\right) \tag{2}$$

3.1.3 Energy Equation

$$\frac{\partial}{\partial x_j}(\overline{u}_i\overline{T}) = \frac{\partial}{\partial x_j}\left[\alpha\left(\frac{\partial \overline{T}}{\partial x_j}\right)\right] + \frac{1}{\rho c_p}\frac{\partial}{\partial x_j}\left(-\rho c_p\overline{u}_j'\overline{T}'\right) \tag{3}$$

3.1.4 Turbulence k-ε Equations

$$\frac{\partial}{\partial x_j}(\rho k u_j) = \frac{\partial}{\partial x_j}\left[\left(\mu + \frac{\mu_t}{\sigma_k}\right)\frac{\partial k}{\partial x_j}\right] + G_k - \rho\varepsilon + S_k \tag{4}$$

$$\frac{\partial}{\partial x_j}(\rho\varepsilon u_j) = \frac{\partial}{\partial x_j}\left[\left(\mu + \frac{\mu_t}{\sigma_\varepsilon}\right)\frac{\partial \varepsilon}{\partial x_j}\right] + C_{1\varepsilon}\frac{\varepsilon}{k}G_k - C_{2\varepsilon}\rho\frac{\varepsilon^2}{k} - S_\varepsilon \tag{5}$$

Turbulence viscosity can be represented as follows [20].

$$\mu_t = \rho C_\mu \frac{k^2}{\varepsilon} \tag{6}$$

Here, $C_{1\varepsilon}$ and $C_{2\varepsilon}$ are constant coefficients, σ_k is turbulence Prandtl number for turbulence kinetic energy equation, and σ_ε is turbulence Prandlt number for turbulence kinetic energy dissipation. These coefficients are constant values obtained after experimental studies and are represented below [20].

$$C1 = 1.44 \quad C2 = 1.92 \quad C_\mu = 0.09 \quad \sigma_k = 1.00 \quad \sigma_\varepsilon = 1.30$$

3.2 Boundary Conditions

The boundary conditions at the boundary points of the solution regions are required to solve the fundamental equations of this problem. In this study, there are two different flows namely primary flow and secondary flow. Therefore, there are 2 "inlet" boundary conditions. Primary flow had constant temperature and uniform velocity and enters from channel inlet. On the other hand, secondary flow was send at constant velocity and uniform temperature in terms of impinging jet impinging on channel upper surfaces. At the exit of the channel, "outlet" boundary conditions were determined and at this surface, changes of all variables were accepted significantly small that could be ignored. All solid surfaces of the channel were accepted isolated and "wall" boundary condition in CFD software was used. Cube surfaces within the channel were accepted to have constant temperature and "wall" boundary condition was used. Based on these assumptions, determined boundary conditions were given below.

3.2.1 Channel input

Air enters the channel under uniform velocity profile

https://doi.org/10.1017/jmech.2018.11 Published online by Cambridge University Press

and constant temperature.

$$u = U_c \quad v = 0 \quad w = 0 \quad T = T_o$$

Turbulence kinetic energy and turbulence kinetic energy dissipation values at the channel entrance can be determined from the following statements [20].

$$k = \frac{3}{2}(U_{ref} T_i)^2 \quad \varepsilon = C_u^{3/2} \frac{k^{3/2}}{l}$$

Here,

$$I = 0.07L \tag{7}$$

T_i represents turbulence density and L represents characteristic length.

3.2.2 Channel Output

At the channel output, the changes in all variables are omitted due to extremely low values.

$$\frac{du}{dx} = 0 \quad \frac{dv}{dx} = 0 \quad \frac{dw}{dx} = 0 \quad \frac{dT}{dx} = 0 \quad \frac{dk}{dx} = 0 \quad \frac{d\varepsilon}{dx} = 0$$

3.2.3 Channel Top Surface

There are two different boundary regions on the top surface of the channel. The top surface of the channel is isolated. The air input is supplied from a nozzle in the middle of this surface.

Top surface (except nozzle)

$$u = 0 \quad v = 0 \quad w = 0 \quad \frac{dT}{dy} = 0 \quad k = 0 \quad \varepsilon = 0$$

On nozzle

$$u = 0 \quad v = V_j \quad w = 0 \quad k = \frac{3}{2}(U_{ref} T_i)^2 \quad \varepsilon = C_\mu^{3/2} \frac{k^{3/2}}{l}$$

3.2.4 Channel Bottom and Side Surfaces

Similarly, there is a wall boundary condition on the channel bottom surface and this surface is isolated.

$$u = 0 \quad v = 0 \quad w = 0 \quad \frac{dT}{dy} = 0 \quad k = 0 \quad \varepsilon = 0$$

3.2.5 On Cube Surfaces

$$u = 0 \quad v = 0 \quad w = 0 \quad T = T_b \quad k = 0 \quad \varepsilon = 0$$

Here T_b represents cube temperature. This value is considered constant at 70°C in all simulations. To represents the temperature of the primary air from channel input and secondary air from nozzle and this selected as 20°C constant temperature.

3.3 Calculation of Nusselt Number

Expression of calculation of Nusselt number is given as follows.

$$Nu = \frac{hD_h}{k} \tag{8}$$

Here, h, k and D_h are heat convection coefficient, fluid thermal conduction coefficient, and hydraulic diameter respectively. Cube surface heat flux can be written,

$$q'' = h(T_w - T_o) = -k \left.\frac{\partial T}{\partial n}\right|_{n=0} \tag{9}$$

Based on Eq. 9, if heat convection coefficient (h) is obtained, the following equation could be constructed.

$$h = -\frac{k}{(T_w - T_o)} \left.\frac{\partial T}{\partial n}\right|_{n=0} \tag{10}$$

If this equation above is written in general formula of Nusselt number, Nusselt number can be obtained.

$$Nu_x = \frac{hD_h}{k} = -\frac{D_h}{(T_w - T_o)} \left.\frac{\partial T}{\partial n}\right|_{n=0} \tag{11}$$

To calculate average Nusselt number, local Nusselt number is integrated through area, and divided into total cube surface are to obtain the following equation.

$$N\bar{u}_A = \frac{1}{A}\int_A Nu_x dA \tag{12}$$

4. NUMERICAL METHOD

The numerical investigation of flow and heat transfer characteristics of the problem depends on solving the differential equations using the appropriate boundary conditions. For the solution of these equations, package program was used. This program is CFD software based on finite volume method operating principle. This method is commonly used for fluid mechanics and heat transfer analysis. Differential equations of the problem were covered within time independent, turbulences, three-dimensional, and incompressible flow. For this purpose, continuity, momentum, and energy equations were determined and k-epsilon equation was selected for turbulence equation. The flow is considered as incompressible and the related pressure-based equations are solved. Before starting numerical analysis, optimum mesh structure was determined, and validity of the solution method was testes with help of literature. Differential equations of the problem were solved with determined boundary conditions. During simulation, convergence criteria were determined as 10^{-6} value. Iterations were conducted until the results converged.

Problem mesh system significantly effects numerical solution results and can cause error in calculations. Therefore, results should be independent from mesh structure (grid number). In this study, to determine the optimum mesh structure, analyses with the highest flow velocity is selected as basis and the simulations are iterated for mesh systems with different grid numbers. The results were constant in the mesh structure with 700.000 grid point. Therefore, this value is selected as optimum mesh structure. In the solution region, to achieve better results in cube surfaces where dependent

https://doi.org/10.1017/jmech.2018.11 Published online by Cambridge University Press

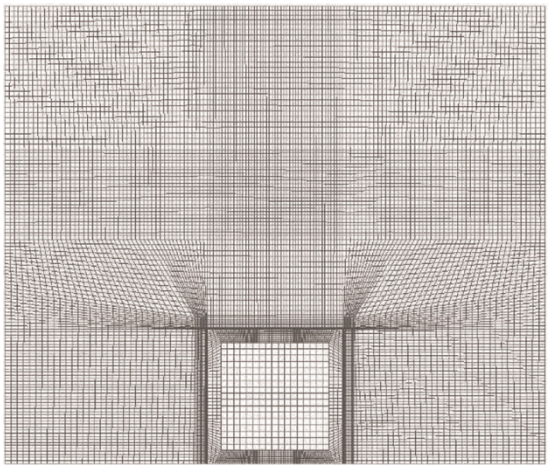


Fig. 2 Mesh structure on x-y axis.

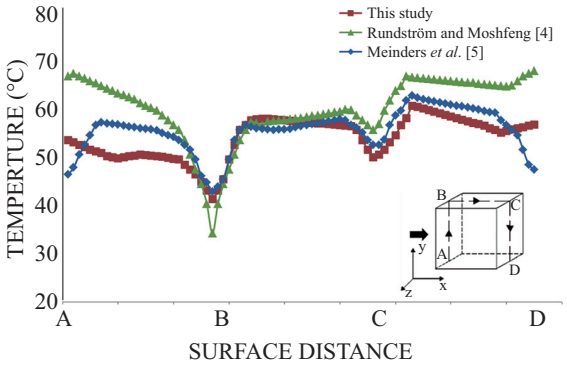


Fig. 3 Comparing temperature changes along the block surface of this study and of Meinders *et al*. [5] and Rundström and Moshfegh [4].

variable (temperature, velocity, pressure etc.) values are constantly changing, mesh density around the surface is increased. The mesh density has higher value in the centre compared to outer surfaces and hexahedral mesh structure is selected where better results for heat convection are obtained. Mesh structure on x-y axis of the problem is shown on Fig. 2.

To approve the validity of the numerical method used for the problem solution, experimental study of Meinders *et al*. [5] and numerical study of Rundström and Moshfegh [4] are selected. For this purpose, simulations are made for the same geometry and boundary conditions and temperature distributions along the cube surfaces are compared. Geometric dimensions and boundary conditions of related studies were not covered here due to length of this information. The results of this study and other two studies are compared in Fig. 3. As the figure indicates, curves for all three studies follow a similar profile. Data obtained in this study have similar results to other studies in terms of cube upper surface (BC), and back surface (CB). However, when the cube contacts with flow, there are differences for draw curves on the front surface of the cube (AB) which is the first region. However, data of this study has similar results with experimental study of Meinders *et al*. [5]. Results of experimental study and simulations showed approximately 5-6°C difference for the front part of the cube. This could be caused by sensitivity and calibration of the measurements during experimental study or numerical errors during simulation study. Yet, in general sense, the results of the three studies are compatible. Thus, it could be said that the numerical methodology adopted in this study has adequate accuracy.

5. FINDINGS AND DISCUSSION

In this study, cooling of a constant temperature cube that represents electronic components inserted inside a channel are investigated. For this purpose, primary air with constant velocity is transferred from channel input, and secondary air with imping jet is transferred to channel upper surface which corresponds to top part of the components. The flows are in contact with the cube that has constant temperature of 70°C and effects the thermal boundary layer on the cube surfaces to create a heat transfer from cube to fluid.

This situation is simulated for constant problem geometry under turbulence conditions for different values of nozzle jet input velocity and channel input velocity ratio V_j/U_c = 1, 2, and, 3 using Reynolds number between 30000-90000 based on channel input velocity. The simulation results are evaluated below.

As stated earlier, there are numerous studies in literature considering only primary or secondary flow. When the channel geometry of only primary flow was investigated, it was observed that generally, fluid had entered the channel with uniform velocity distribution, boundary layer was disrupted by hit to cube, and the fluid passes above the cube and generated circulation regions at the back of the cube. This disruption in boundary layer plays an important role on heat transfer from cube to fluid. Yet, as in this study, additional secondary fluid again disrupts existing flow structure. The effects of using primary and secondary flows together on flow and heat transfer were given below.

When Reynold number is selected as 30000 in Figs. 4, 5, and 6, for nozzle input velocity and channel input velocity ratio of (V_j/U_c) 1, 2, and 3 respectively, velocity vector distributions are given for the surrounding of heat dissipating cube. When the figures are investigated, flow structure of impinging jet and channel cross flows are clear. Here, primary air with constant velocity from channel input impinges to left surface of the cube, the velocity of the air decreases in this region, but the velocity of the air increases on the top surface of the cube and moves towards the channel output. At the same time, secondary air with imping jet is transferred to channel upper surface which corresponds to top part of the components. This secondary air is moving from the top surface of the cube in vertical direction. However, primary and secondary airs encounter in certain regions and effect the velocity and flow direction of each other. This situation is similar for all 3 figures.

In Fig. 4 for velocity vector distribution for Reynolds number = 30000 and V_j/U_c = 1 can be observed. In this figure velocity of primary and secondary flows are equal.

https://doi.org/10.1017/jmech.2018.11 Published online by Cambridge University Press

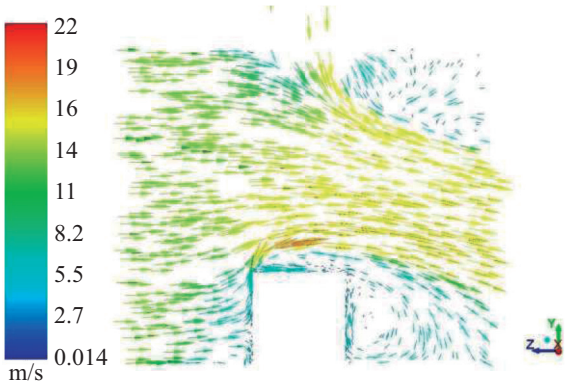


Fig. 4 Velocity vector distribution for Reynolds number = 30000 and $V_j/U_c = 1$.

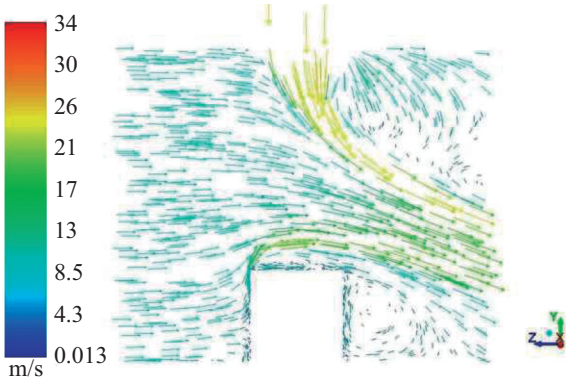


Fig. 5 Velocity vector distribution for Reynolds number = 30000 and $V_j/U_c = 2$.

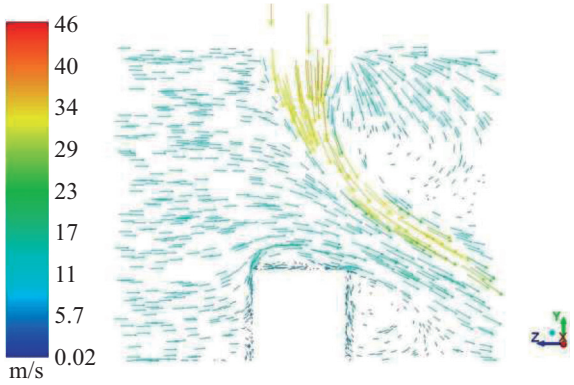


Fig. 6 Velocity vector distribution for Reynolds number = 30000 and $V_j/U_c = 3$.

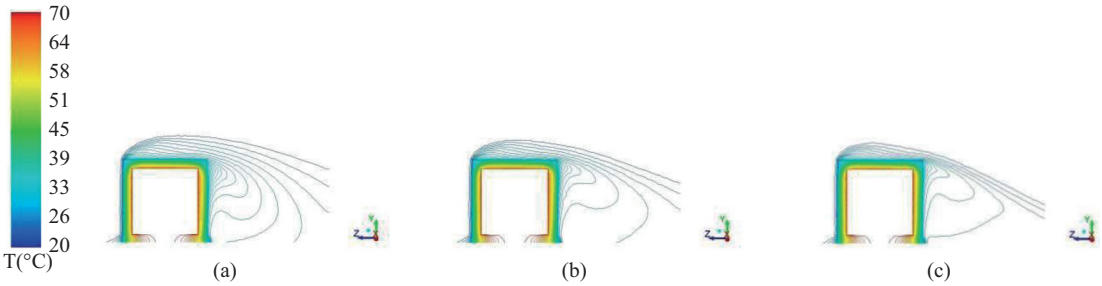


Fig. 7 Temperature contours for Reynolds number = 30000 (a) $V_j/U_c = 1$, (b) $V_j/U_c = 2$, (c) $V_j/U_c = 3$.

As the figure suggests, the effect of primary flow is more dominant. Flow around the cube has similar structure with the channel cross flow characteristics. Primary flow that has constant velocity at the channel input, horizontally accelerates and impinges to the cube. Velocity vectors on the left side of the cube decreases and the vectors on the top of the cube increases. As the back of the cube, velocity vectors change direction and create a circulation region. Secondary flow from the nozzle on the top surface cannot reach to the cube surface. Yet this flow, applies pressure on the primary flow from the top, compresses flow lines, and effects the thickness of velocity boundary layer on the cube surface.

When Figs. 5 and 6 are investigates increase in V_j/U_c ratio effects the vector distribution of the flow. This increase leads to increase the effect of secondary flow on the flow characteristic of the problem. As the figures suggest, primary flow is more effective on the left side of the cube. However, in other regions, the effect of secondary flow increases in line with V_j/U_c ratio. This ratio increases changes when primary and secondary flows are merges. Therefore, the flow lines on the top surface of the cube are thicker. Additionally, the flow direction of the secondary flow approaches to lefts side and by changing the direction and intensity of the velocity vectors on the right side of the cube, this flow increases the intensity of the circulation.

When Reynold number is selected as 30000 in Fig. 7,

https://doi.org/10.1017/jmech.2018.11 Published online by Cambridge University Press

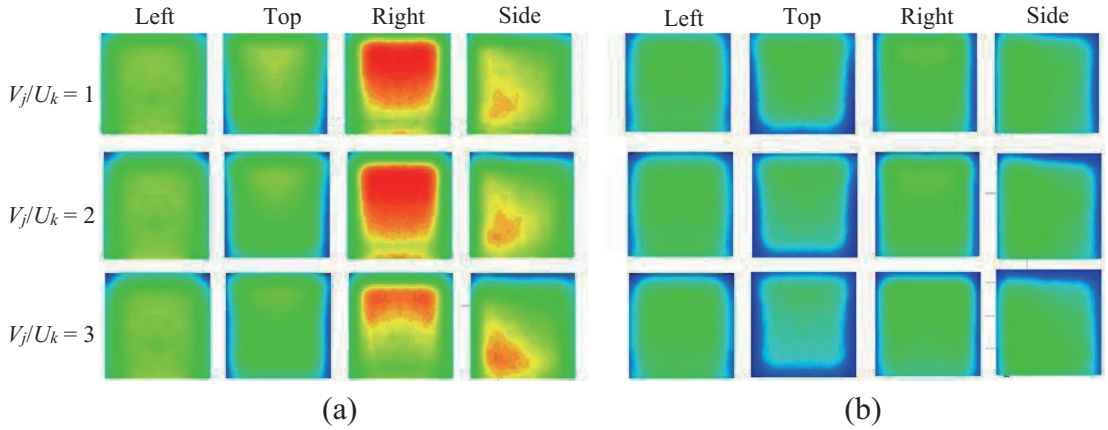


Fig. 8 Temperature distribution of heat generating cube surface for different V_j/U_c ratio (a) Re = 30000, (b) Re = 90000.

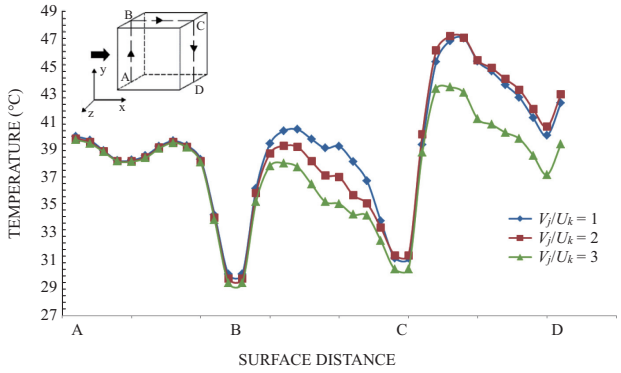


Fig. 9 Local temperature changes along the left, top, and right-side surfaces of the cube when Reynolds number 30000.

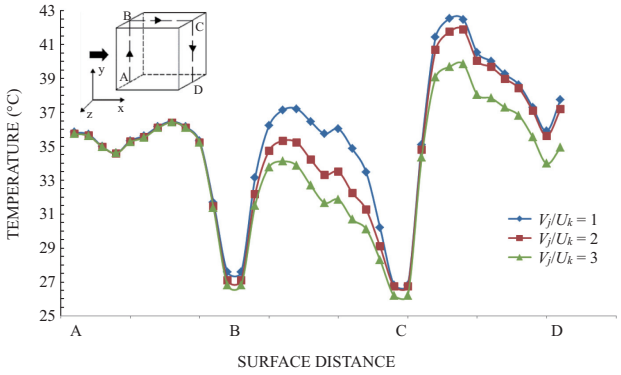


Fig. 10 Local temperature changes along the left, top, and right side surfaces of the cube when Reynolds number 60000.

for nozzle input velocity and channel input velocity ratio of (V_j/U_c) 1, 2, and 3 respectively, temperature contours are given for the surrounding of heat dissipating cube. When the figure is investigated, similar structure is observed for V_j/U_c ratio. Primary air that has low temperature at the channel input, impinges the high temperature cube and heat transfer occurs on the cube surface. Meanwhile, secondary air is effective on the top surface of the cube with lower temperature and merges with the primary air to create heat transfer on the top and right-side surfaces of the cube. As V_j/U_c ratio increases, change of heat boundary layer in flow region is observed. This change is clear on the top and right-side surface of the cube. The reason for this situation is thermal boundary layer breaks down as secondary flow had significant effect on general structure of the flow and high V_j/U_c ratio. When this situation occurs, this leads to enhancement on heat transfer.

For different values of nozzle jet input velocity and channel input velocity ratio (V_j/U_c), when Reynolds numbers are 30000 and 90000 respectively, temperature distributions of the left, top, right, and side (side surfaces of the cube in +z and -z directions) of the heat dissipating cube are indicated in Fig. 8.

As the problem is symmetrical on z axis, +z and -z temperature distributions are similar. Therefore, only one of the two surfaces is included in the figure. Temperature distributions on these two surfaces and on the left surface of the cube are not significantly affected from V_j/U_c ratio. The reason is primary flow is more dominant on the flows in this region. Temperature on the top and right surface of the cube is changing in line with V_j/U_c ratio. Especially, on the right surface there is a significant change. The reason is in this region, secondary flow has more dominant role, the flow effects on the general structure of the flow, the flow contributes to circulation inside the flow, and increased heat transfer by disturbing the boundary layer. This situation is observed in all Reynolds numbers.

In Figs. 9, 10, and 11, when the Reynolds numbers are 30000, 60000, and 90000 respectively, local temperature changes on the left, top, and right-side surfaces of the cube are indicated for different V_j/U_c ratio. When the figures are investigated, for all Reynolds numbers and V_j/U_c ratio, the curves have similar structure. In the first contact with primary flow, local temperature values

https://doi.org/10.1017/jmech.2018.11 Published online by Cambridge University Press

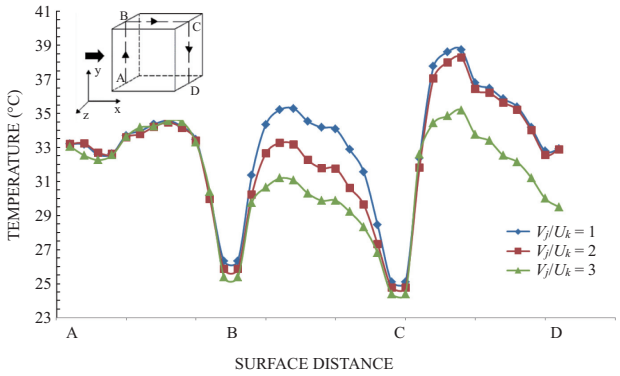


Fig. 11 Local temperature changes along the left, top, and right-side surfaces of the cube when Reynolds number 90000.

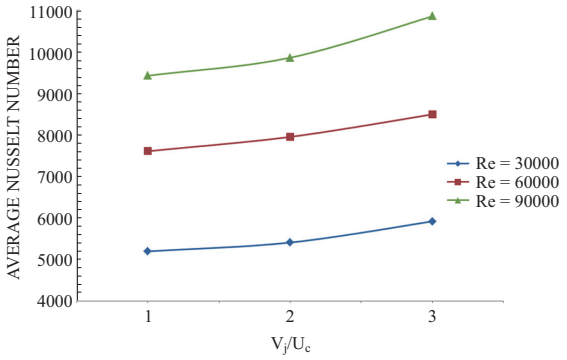


Fig. 12 Change in Average Nusselt numbers and V_j/U_c ratio for different Reynolds.

on most of the AB surface have similar values. However, local temperature values decrease at the B point on the upper left corner of the heat dissipating cube and reaches to minimum value on point B. The reason is as the primary flow contacts with cube surfaces, fluid velocities have the minimum value of point B and there can be splits at the velocity boundary layers of this region. On the top surface of the clock, temperature slightly increases on the flow direction, yet, decreases at point C. At point C, second minimum value is achieved. Second minimum value is highly effected from the secondary flow of the impinging jet near point C. The primary is suppressed by the secondary flow and at point C, the boundary layer is disrupted. Therefore, heat transfer on the heat dissipating cube may increase. From point C, local temperatures show a sudden increase and reaches to maximum value and then along CD surface, the temperatures decrease.

For all 3 figures, Reynolds number is kept constant and as the nozzle jet input velocity and channel input velocity ratio (V_j/U_c) increases, this situation is effective on the local temperature values. However, such effect is not visible along AB surface. For all three Reynolds numbers, curves for different V_j/U_c ratio along the surfaces overlap. The reason is the effect of primary flow is more effective on general flow on this surface and V_j/U_c ratio has insignificant effect on the primary flow in this region.

Along BC surface, curves for different V_j/U_c ratio are different. The reason is both primary and secondary flows are effective on the general structure of the flow on the top surface of the cube. The change in V_j/U_c ratio directly effects secondary flow generation. Therefore, general flow structure in this reason changes. As the figures suggest, as V_j/U_c ratio increases, local temperature values along BC surface decreases. Therefore, as V_j/U_c ratio increases, it can be said that heat transfer along the upper surface of the cube increases and this situation plays an important role on cooling.

Similarly, along CD surface, curves for different V_j/U_c ratio are different. The reason for this situation is the dominant role of secondary flow on the general flow structure in this region. Impinging jet from nozzle supresses fluid that flows on the cube due to primary flow. This suppression causes flow structure deformations on the areas that are close to surface of the cube. This situation supports the circulation at the back side of the cube, effects the boundary layer in this region, and slightly increases the heat transfer. As the figures suggest, as V_j/U_c ratio increases, local temperature values along CD surface decreases. Therefore, as V_j/U_c ratio increases, it can be said that heat transfer along the upper surface of the cube increases.

Figure 12 shows the change in average Nusselt numbers, and V_j/U_c ratio with different Reynolds numbers. As seen from the figure, the increase in Reynolds number, increase average Nusselt number value for each V_j/U_c ratio. The reason is in line with increased fluid velocities, convection heat transfer on the cube surfaces increase. If the figure is analysed for constant Reynolds numbers, as the nozzle jet input velocity and channel input velocity ratio (V_j/U_c) increases, average Nusselt number increases as well. This situation occurs as V_j/U_c ratio increases, secondary flow has more effective role on the general structure of the flow. This increase changes the direction and intensity of the velocity vectors on the top and right-side surfaces of the cube, contributes to circulation and inverse flow regions, and therefore, positively effects heat transfer by changing boundary layers.

6. CONCLUSIONS

In this study, cooling of a constant temperature cube that represents electronic components inserted inside a channel are investigated. For this purpose, primary air with constant velocity is transferred from channel input, and secondary air with imping jet is transferred to channel upper surface which corresponds to top part of the components. The flows are in contact with the cube that has constant temperature and effects the thermal boundary layer on the cube surfaces to create a heat transfer from cube to fluid. The results of the simulations show that the effect of secondary flow is insignificant for the left surface of the cube and primary flow had dominant role to generate general flow. On the top and right side of the cube, both primary and secondary flows are effective. However, in these regions, as the nozzle jet input velocity and channel input velocity ratio (V_j/U_c)

https://doi.org/10.1017/jmech.2018.11 Published online by Cambridge University Press

increases, the effect of secondary flow increases. The secondary flow due to impinging jet directs the primary flow parallel to the channel axis towards the cube surfaces, effects boundary layers, and positively contributes to heat transfer. In addition, as Reynolds number increases, these higher values play significant role to increase the convectional heat transfer on the cube surfaces.

Thus, using the combination of impinging jet and channel cross flow, the thermal components of an electronic circuit can be kept in the safe operating temperatures. The reason is as all the components are cooled to a certain temperature using the primary flow, and the high thermal load components are cooled with the support of impinging jet application, heat transfer from the components to fluid can be increased and this operation can contribute to cooling.

In this study, fluid was selected as air. The effects of different fluid types on flow and thermal characteristics are not considered. Literature review presents that there are studies on cooling with nanofluids [21, 22]. However, there was no study with nanofluids in case of cooling with cross flow and jet combination. In the future, researchers may focus on effects of nanofluids.

NOMENCLATURE

C_p	specific heat, J/(kg K)
$C_{1\varepsilon}$	constant coefficient 1
$C_{2\varepsilon}$	constant coefficient 2
D	jet diameter, (m)
H	channel height, (m)
h (1)	side length of the cube, (m)
h (2)	heat convection coefficient
k	turbulence flow kinetic energy, (J)
L	characteristic length
Nu	Nusselt number
Nu_x	local Nusselt number
Re_c	channel Reynolds number
T_c	channel air input temperature, (°C)
T_i	turbulence density
T_j	nozzle air input temperature, (°C)
T_o	fluid input temperature (°C)
T_w	cube surface temperature (°C)
U_c	channel flow speed, (m/s)
V_j	jet flow speed, (m/s)
μ	dynamic viscosity of air, (kg/ms)
λ	thermal conductivity, (W/mK)
σ_k	turbulence Prandtl number for turbulence kinetic energy equation
σ_ε	turbulence Prandlt number for turbulence kinetic energy dissipation
q''	heat flux, (W/m^2)

REFERENCES

1. Hajmohammadi, M. R., "Optimal Design of Tree-Shaped Inverted Fins," *International Journal of Heat and Mass Transfer,* **116**, pp. 1352-1360 (2018).
2. Hajmohammadi, M. R., "Introducing a ψ-Shaped Cavity for Cooling a Heat Generating Medium," *International Journal of Thermal Sciences,* **121**, pp. 204-212 (2017).
3. Hajmohammadi, M. R., "Design and Analysis of Multi-Scale Annular Fin Attached to a Pin Fin," *International Journal of Refrigeration* (2018).
4. Rundstrom, D. and Moshfegh, B., "Investigation of Flow and Heat Transfer of an Impinging Jet in a Cross-Flow for Cooling of a Heated Cube," *Journal of Electronic Packaging*, **2**, pp. 150-157 (2006).
5. Meinders E. R., Van Der Meer, T. H. and Hanjalic, K., "Local Convective Heat Transfer from an Array of Wall-Mounted Cubes," *International Journal of Heat and Mass Transfer*, pp. 335-346 (1998).
6. Lee, J. and Lee, S. J., "Stagnation Region Heat Transfer of a Turbulent Axisymmetric Jet Impingement," *Experimental Heat Transfer*, **156**, pp. 137-156 (2010).
7. Mergen, S., "Numerical Investigation of Cooling of an Electronic Component with Crossflow and Impinging Jet," M. S. Thesis, Department of Mechanical Engineering, Gazi University, Ankara, Turkey (2014).
8. Ostheimer, D. and Yang, Z., "A CFD Study of Twin Impinging Jets in a Cross-Flow," *The Open Numerical Methods Journal*, **4**, pp. 24-34 (2012).
9. Guoneng, L., Zhihua, X., Youqu, Z., Wenwen, G. and Cong, D., "Experimental Study on Convective Heat Transfer from a Rectangular Flat Plate by Multiple Impinging Jets in Laminar Cross Flows," *International Journal of Thermal Sciences*, **108**, pp. 123-131 (2016).
10. Hayee, M. W., Tekasakul, P., Eiamsa-ard, S. and Nuntadusit, C., "Flow and Heat Transfer Characteristics of In-Line Impinging Jets With Cross-Flow At Short Jet-To-Plate Distance," *Experimental Heat Transfer*, **28**, pp. 511-530 (2015).
11. Qi, M., Chen, Z. and Fu, R., "Flow Structure of the Plane Turbulent Impinging Jet in Cross Flow," *Journal of Hydraulic Research*, **39**, pp. 155-161 (2001)
12. Rundström, D. and Moshfegh, B., "Large-Eddy Simulation of an Impinging Jet in a Cross-Flow on a Heated Wall-Mounted Cube," *International Journal of Heat and Mass Transfer*, **52**, pp. 921-931 (2009).
13. Popovac, M. and Hanjalic, K., "Large-Eddy Simulations of Flow over a Jet-Impinged Wall-Mounted Cube in a Cross Stream," *International Journal of Heat and Fluid Flow*, **28**, pp. 1360-1378 (2007).
14. Chiang, K. T., "Modeling and Optimization of Designing Parameters for a Parallel-Plain Fin Heat Sink with Confined Impinging Jet Using The

https://doi.org/10.1017/jmech.2018.11 Published online by Cambridge University Press

Response Surface Methodology," *Applied Thermal Engineering*, **27**, pp. 2473-2482 (2007).

15. Maghrabie, H. M., Attalla, M., Fawaz, H. E. and Khalil, M., "Numerical Investigation of Heat Transfer and Pressure Drop of In-Line Array of Heated Obstacles Cooled by Jet İmpingement in Cross-Flow," *Alexandria Engineering Journal*, **56**, pp. 285-296 (2017).
16. Heo, M. W., Lee, K. D. and Kim, K. Y., "Optimization of an Inclined Elliptic Impinging Jet with Cross Flow for Enhancing Heat Transfer," *Heat Mass Transfer*, **47**, pp. 731-742 (2011).
17. Shapiro, S., King, J., Karagozian, A. and M'Closkey, R., "Optimization of Controlled Jets in Crossflow," *41st AIAA Aerospace Sciences Meeting and Exhibit*, Reno, Nevada (2003).
18. Yakhot, A., Liu, H. and Nikitin, N., "Turbulent Fow around a Wall-Mounted Cube: A Direct Numerical Simulation," *International Journal of Heat and Fluid Flow*, **27**, pp. 994-1009 (2006).
19. Popovac, M and Hanjalic, K., "Vortices and Heat Flux around a Wall-Mounted Cube Cooled Simultaneously by a Jet and a Crossflow," *International Journal of Heat and Mass Transfer*, **52**, pp. 4047-4062 (2009).
20. Malalasekera, W. and Versteeg, H. K., *An Introduction to Computational Fluid Dynamics, The Finite Volume Method*, Longman (2005).
21. Hajmohammadi, M. R., "Assessment of a Lubricant Based Nanofluid Application in a Rotary System," *Energy Conversion and Management*, **146**, pp. 78-86 (2017).
22. Hajmohammadi, M. R., "Cylindrical Couette Flow and Heat Transfer Properties of Nanofluids; Single-Phase and Two-Phase Analyses," *Journal of Molecular Liquids*, **240**, pp. 45-55 (2017).

(Manuscript received September 19, 2017,
accepted for publication February 12, 2018.)

https://doi.org/10.1017/jmech.2018.11 Published online by Cambridge University Press